整理NO.	分野	特許概要	想定応用製品	期待効果	酸化チタンの大きさ	酸化チタンの用法	製品例	関係 http	公開・公表番号	出願人	発明等の名称
63	洗浄剤	紫外光の乏しい屋内において、通常照明用に用いられる昼白色蛍光灯の光で高い抗菌活性を示す抗菌性付与剤である。二酸化チタンと酸性物質および／またはその塩とから生成する二酸化チタン複合体を含有する抗菌性付与剤とする。二酸化チタン複合体は、二酸化チタンに酸性物質および／またはその塩を含浸、吸着もしくは混合させるか、あるいはチタン化合物の水溶液と酸性物質および／またはその塩の水溶液を共沈殿させることにより得られる。酸性物質および／またはその塩は、硫酸、タングステン酸、硫酸アンモニウム、硫酸チタン、タングステン酸アンモニウムまたはタングステン酸チタンから選ばれる。	食器などの除菌	抗菌	―				2006-131583	丸勝産業株式会社	抗菌性付与剤
64	水浄化	水浄化装置は、処理水を通過させる反応容器と、反応容器内に配置された光触媒機能を有する繊維の不織布からなる成形物と、成型物に紫外線を照射するように反応容器に配置された紫外線 LED ユニットとからなる水浄化装置である。光触媒機能を有する繊維は、シリカ成分を主体とする酸化物相（第 1 相）とチタンを含む金属酸化物相（第 2 相）との複合酸化物からなる繊維であつて、第 2 相を構成する金属酸化物のチタンの存在割合が繊維の表層に向かつて傾斜的に増大している。	飲料水	抗菌	―	繊維と混合	アクアソリューション(2013年10月で販売中止)	http://www.ube-ind.co.jp/japanese/news/2006/2006_37.htm	2012-200672	宇部興産株式会社	水浄化装置
65	水浄化	二酸化チタン超微粒子を、石英微粒子の表面上に固定化させ、固定化二酸化チタンと被処理水を含む懸濁液に紫外光を照射し、ハイドロサイクロンで固定化二酸化チタンを回収することにより、水中の有機不純物を分解する光触媒反応の効率と、固液分離の効率を両立させる。担持微粒子は、大きさが 5μm 以上 30μm 以下の石英から成る微粒子で、大きさが 10nm 程度の二酸化チタン超微粒子を用いる。	飲料水	光触媒	ナノ	10nm のアナターゼ型二酸化チタンを石英微粒子に担持		http://panasonic.co.jp/corp/news/official.data/data.dir/2013/08/jn130805-6/jn130805-6.html	2012-254425	パナソニック株式会社	複合化光触媒による水浄化技術
66	水浄化	光触媒機能被膜は、二酸化チタンを含む微粒子、好ましくは、アパタイト、ゼオライトおよび活性炭からなる群より選択される吸着剤と、二酸化チタンとを、1：99～7：93 の質量比で含有する混合物を原料粉として、フレーム温度 700～2000℃の高速フレーム溶射により形成される。	飲料水	光触媒	―	焼結			2008-194616	株式会社フジコー，国立大学法人九州大学	光触媒機能皮膜およびそれを用いた水処理方法

＜酸化銀と酸化チタンの使用実態調査における引用文献＞

[i] Scientific Committee on Emerging and Newly Identified Health Risks(SCENIHR)、Preliminary Opinion、Nanosilver: safety, health and environmental effects and role in antimicrobial resistance、SCENIHR approved this opinion at the 4th plenary of 12 December 2013、p8

[ii] https://www.silverinstitute.org/site/silver-in-technology/silver-in-green/water-purification-anti- bacterial/

[iii] 特開 2006-281023(東レ株式会社)

[iv] The National Institute for Public Health and the Environment (RIVM)、Exposure to nanomaterials in consumer products、RIVM Letter Report 340370001/2009、p19

[v] SNWG submission to NIOSH-Silver Nanoparticles (AgNPs); Information and Comment Request / February 2013 (https://www.silverinstitute.org/site/wp-content/uploads/2013/05/SNWG_SKMBT2013.pdf)

[vi] Scientific Committee on Emerging and Newly Identified Health Risks(SCENIHR)、Preliminary Opinion Nanosilver: safety, health and environmental effects and role in antimicrobial resistance SCENIHR approved this opinion at the 4th plenary of 12 December 2013、p21

[vii] 抗菌加工製品の内外市場に関する調査研究（2004 年 9 月）、http://www.meti.go.jp/policy/mono_info_service/mono/human-design/koukin.html

[viii] Bernd Nowack,, Harald F. Krug, Murray Height、Environmental Science & Technology、Vol. 45, p1177-1183(2011)

[ix] MARTINEZ-ABAD Antonio, LAGARON Jose M., OCIO Maria J. 、Journal of Agricultural Food Chemistry、Vol.60, No.21, p.5350-5359 (2012)

[x] Marina E. Quadros, Linsey C. Marr、Environmental Science & Technology、Vol.45 (24), p 10713–10719(2011)

[xi] Nanomaterial in consumer products Detection, characterisation and interpretation RIVM Report 320029001/2011, The National Institute for Public Health and the Environment (RIVM), p53(2011)

[xii] http://www.nanotechproject.org/cpi/ (2014 年 2 月 5 日アクセス)

[xiii] GOETZ Natalie von, FABRICIUS Lars, GLAUS Reto, WEITBRECHT Volker, GUENTHER Detlef, HUNGERBUEHLER Konrad、Food Additives & Contaminants Pt A Chemistry Analysis Control Expo Risk Assess、Vol.30, No.3, p612-620 (2013)

[xiv] EMAMIFAR Aryou, KADIVAR Mahdi, SHAHEDI Mohammad, SOLEIMANIANZAD Sabihe 、Food Control、Vol.22 No.34,p.408-413 (2011)

[xv] M. Cushen, J. Kerry, M. Morris, M. Cruz-Romero, E. Cummins、Journal of Agricultural and Food Chemistry、Vol.62 (6), p1403–1411(2014)

[xvi] 福田淳、生産と技術、Vol.66, No.1 p54-59 (2014)

[xvii] Regulation (EC) No 1333/2008 http://eur-lex.europa.eu/LexUriServ/LexUriServ.do?uri=CONSLEG:2008R1333:20131014:EN:PDF (Consolidated versions, 2013 年 10 月 14 日版)

[xviii] WEIR Alex, WESTERHOFF Paul, FABRICIUS Lars, VON GOETZ Natalie, FABRICIUS Lars、Environmental Science & Technology、Vol.46, No.4, p2242-2250 (2012)

[xix] Xin-Xin Chen , Bin Cheng , Yi-Xin Yang , Aoneng Cao , Jia-Hui Liu , Li-Jing Du ,Yuanfang Liu , Yuliang Zhao , Haifang Wang 、Small、Vol. 9, No. 9-10, p1765-1774 (2013)

[xx] http://www.merck-performance-materials.com/en/candurin/candurin_for_food /candurin_for_food.html

[xxi] http://www.merck-performance-materials.com/merck-ppf/detailRequest?source=PRONET&docId= 201111.003

[xxii] PETER Anca, NICULA Camelia, MIHALY-COZMUTA Anca, MIHALY-COZMUTA Leonard, INDREA Emi、International Journal of Food Science & Technology、Vol.47, No.7, p1448-1456(2012)

[xxiii] Systemic Absorption of Nanomaterials by Oral Exposure : Part of the "Better control of nano" initiative 2012-2015. – Annual report year: 2013. (http://www2.mst.dk/Udgiv/publications/2013/09/978-87-93026-51-3.pdf)

[24] Scientific Committee on Emerging and Newly Identified Health Risks(SCENIHR)、Preliminary Opinion、Nanosilver: safety, health and environmental effects and role in antimicrobial resistance、SCENIHR approved this opinion at the 4th plenary of 12 December 2013、p8

[25] https://www.silverinstitute.org/site/silver-in-technology/silver-in-green/water-purification-anti- bacterial/

[26] 特開 2006-281023(東レ株式会社)

[27] The National Institute for Public Health and the Environment (RIVM)、Exposure to nanomaterials in consumer products、RIVM Letter Report 340370001/2009、p19

[28] SNWG submission to NIOSH-Silver Nanoparticles (AgNPs); Information and Comment Request / February 2013 (https://www.silverinstitute.org/site/wp-content/uploads/2013/05/SNWG_SKMBT2013.pdf)
[29] Scientific Committee on Emerging and Newly Identified Health Risks(SCENIHR)、Preliminary Opinion Nanosilver: safety, health and environmental effects and role in antimicrobial resistance SCENIHR approved this opinion at the 4th plenary of 12 December 2013、p21
[30] 抗菌加工製品の内外市場に関する調査研究（2004 年 9 月）、 http://www.meti.go.jp/policy/mono_info_service/mono/human-design/koukin.html
[31] Bernd Nowack,, Harald F. Krug, Murray Height、Environmental Science & Technology、Vol. 45, p1177-1183(2011)
[32] MARTINEZ-ABAD Antonio, LAGARON Jose M., OCIO Maria J. 、Journal of Agricultural Food Chemistry、Vol.60, No.21, p.5350-5359 (2012)
[33] Marina E. Quadros, Linsey C. Marr、Environmental Science & Technology、Vol.45 (24), p 10713–10719(2011)
[34] Nanomaterial in consumer products Detection, characterisation and interpretation RIVM Report 320029001/2011, The National Institute for Public Health and the Environment (RIVM), p53(2011)
[35] http://www.nanotechproject.org/cpi/ (2014 年 2 月 5 日アクセス)
[36] GOETZ Natalie von, FABRICIUS Lars, GLAUS Reto, WEITBRECHT Volker, GUENTHER Detlef, HUNGERBUEHLER Konrad、Food Additives & Contaminants Pt A Chemistry Analysis Control Expo Risk Assess、Vol.30, No.3, p612-620 (2013)
[37] EMAMIFAR Aryou, KADIVAR Mahdi, SHAHEDI Mohammad, SOLEIMANIANZAD Sabihe 、Food Control、Vol.22 No.34,p.408-413 (2011)
[38] M. Cushen, J. Kerry, M. Morris, M. Cruz-Romero, E. Cummins、Journal of Agricultural and Food Chemistry、Vol.62 (6), p1403–1411(2014)
[39] 福田淳、生産と技術、Vol.66, No.1 p54-59 (2014)
[40] Regulation (EC) No 1333/2008 http://eur-lex.europa.eu/LexUriServ/LexUriServ.do?uri=CONSLEG:2008R1333:20131014:EN:PDF (Consolidated versions, 2013 年 10 月 14 日版)
[41] WEIR Alex, WESTERHOFF Paul, FABRICIUS Lars, VON GOETZ Natalie, FABRICIUS Lars、Environmental Science & Technology、Vol.46, No.4, p2242-2250 (2012)
[42] Xin-Xin Chen , Bin Cheng , Yi-Xin Yang , Aoneng Cao , Jia-Hui Liu , Li-Jing Du ,Yuanfang Liu , Yuliang Zhao , Haifang Wang 、Small、Vol. 9, No. 9-10, p1765-1774 (2013)
[43] http://www.merck-performance-materials.com/en/candurin/candurin_for_food_/candurin_for_food.html
[44] http://www.merck-performance-materials.com/merck-ppf/detailRequest?source=PRONET&docId=201111.003
[45] PETER Anca, NICULA Camelia, MIHALY-COZMUTA Anca, MIHALY-COZMUTA Leonard, INDREA Emi、International Journal of Food Science & Technology、Vol.47, No.7, p1448-1456(2012)
[46] Systemic Absorption of Nanomaterials by Oral Exposure : Part of the "Better control of nano" initiative 2012-2015. – Annual report year: 2013. (http://www2.mst.dk/Udgiv/publications/2013/09/978-87-93026-51-3.pdf)

別紙４

研究成果の刊行に関する一覧表

書籍

著者氏名	論文タイトル名	書籍全体の編集者名	書　籍　名	出版社名	出版地	出版年	ページ
	該当なし						

雑誌

発表者氏名	論文タイトル名	発表誌名	巻号	ページ	出版年
Xu J, Futakuchi M, Alexander DB, Fukamachi K, Numano T, Suzui M, Shimizu H, Omori T, Kanno J, Hirose A, Tsuda H.	Nanosized zinc oxide particles do not promote DHPN-induced lung carcinogenesis but cause reversible epithelial hyperplasia of terminal bronchioles.	Arch Toxicol.	88	65-75	2014
Taquahashi, Y, Ogawa, Y, Takagi, A, Tsuji, M, Morita, K, Kanno, J.	An improved dispersion method of multi-wall carbon nanotube for inhalation toxicity studies of experimental animals.	J. Toxicol. Sci.	38	619-628	2013
広瀬明彦	ナノマテリアルの健康影響評価指針の国際動向	薬学雑誌	133	175-180	2013

Arch Toxicol (2014) 88:65–75
DOI 10.1007/s00204-013-1086-5

INORGANIC COMPOUNDS

Nanosized zinc oxide particles do not promote DHPN-induced lung carcinogenesis but cause reversible epithelial hyperplasia of terminal bronchioles

Jiegou Xu · Mitsuru Futakuchi · David B. Alexander · Katsumi Fukamachi · Takamasa Numano · Masumi Suzui · Hideo Shimizu · Toyonori Omori · Jun Kanno · Akihiko Hirose · Hiroyuki Tsuda

Received: 25 February 2013 / Accepted: 20 June 2013 / Published online: 6 July 2013

Abstract Zinc oxide (ZnO) is known to induce lung toxicity, including terminal bronchiolar epithelial hyperplasia, which gives rise to concerns that nanosized ZnO (nZnO) might lead to lung carcinogenesis. We studied the tumor promoting activity of nZnO by an initiation–promotion protocol using human c-Ha-*ras* proto-oncogene transgenic rats (H*ras*128 rats). The rats were given 0.2 % N-nitrosobis(2-hydroxypropyl)amine (DHPN) in the drinking water for 2 weeks and then treated with 0.5 ml of 250 or 500 μg/ml nZnO suspension by intra-pulmonary spraying once every 2 weeks for a total of 7 times. Treatment with nZnO particles did not promote DHPN-induced lung carcinogenesis. However, nZnO dose-dependently caused epithelial hyperplasia of terminal bronchioles (EHTB) and fibrosis-associated interstitial pneumonitis (FAIP) that were independent of DHPN treatment. Tracing the fate of EHTB lesions in wild-type rats indicated that the hyperplastic lesions almost completely disappeared within 12 weeks after the last nZnO treatment. Since nZnO particles were not found in the lung and $ZnCl_2$ solution induced similar lung lesions and gene expression profiles, the observed lesions were most likely caused by dissolved Zn^{2+}. In summary, nZnO did not promote carcinogenesis in the lung and induced EHTB and FAIP lesions that regressed rapidly, probably due to clearance of surplus Zn^{2+} from the lung.

Keywords Nanosized zinc oxide particles · Lung toxicity · Lung carcinogenesis · Epithelial hyperplasia of terminal bronchioles · Interstitial pneumonitis · Lung fibrosis

Electronic supplementary material The online version of this article (doi:10.1007/s00204-013-1086-5) contains supplementary material, which is available to authorized users.

J. Xu · D. B. Alexander · H. Tsuda (✉)
Laboratory of Nanotoxicology Project, Nagoya City University, 3-1 Tanabedohri Mizuho-ku, Nagoya 467-8603, Japan
e-mail: htsuda@phar.nagoya-cu.ac.jp

J. Xu · M. Futakuchi · K. Fukamachi · T. Numano · M. Suzui
Department of Molecular Toxicology, Nagoya City University Graduate School of Medical Sciences, 1-Kawasumi, Mizuho-cho, Mizuho-ku, Nagoya 467-8601, Japan

H. Shimizu
Core Laboratory, Nagoya City University Graduate School of Medical Sciences, 1-Kawasumi, Mizuho-cho, Mizuho-ku, Nagoya 467-8601, Japan

T. Omori
Department of Health Care Policy and Management, Nagoya City University Graduate School of Medical Sciences, 1-Kawasumi, Mizuho-cho, Mizuho-ku, Nagoya 467-8601, Japan

J. Kanno · A. Hirose
National Institute of Health Sciences, 1-18-1 Kamiyoga, Setagaya-ku, Tokyo 158-8501, Japan

Introduction

One of the most widely used nanomaterials is nZnO. The worldwide production of nZnO powder is increasing every year and was reported to have reached 1.4 million tons in 2011. It is used in rubber industry and electronics and in commercial products such as sunscreens and paints. In the biomedical field, it is used in baby powders, antiseptic ointments, and zinc oxide tapes to treat a variety of skin conditions (Baldwin et al. 2001; Hughes and McLean 1988). Recently, nZnO has gained interest in cancer applications or as an active anticancer drug (Rasmussen et al. 2010).

Micron or larger-sized ZnO particles are considered to be "Generally Recognized as Safe" (GRAS) in food

additives by the FDA. However, exposure to fumes containing ZnO and other metal particles during welding or galvanizing processes is known to lead to metal fume fever (Antonini et al. 2003; Drinker and Fairhall 1933; Fine et al. 1997). Recent reports have shown that nZnO affects cell viability and induces reactive oxygen species (ROS) in many mammary cell types in tissue culture (Deng et al. 2009; Lee et al. 2008; Xia et al. 2008; Yang et al. 2009), cause proliferation of airway epithelial cells, goblet cell hyperplasia, interstitial pulmonary inflammation and fibrosis (Cho et al. 2011), and reversible inflammatory reaction in the bronchoalveolar lavage fluid in animal studies (Sayes et al. 2007; Warheit et al. 2009). nZnO also leads to DNA damage (Kermanizadeh et al. 2012) and micronuclei formation in vitro (Valdiglesias et al. 2013). While these in vitro and in vivo studies have provided some information on acute toxic effects of nZnO on certain cell types and animals, further in vivo studies are needed to determine whether nZnO has chronic toxic effects as in some other metal oxide particles. For example, epidemiological data indicate that exposures of aluminum oxide or iron oxide lead to pneumoconiosis in human (Hull and Abraham 2002; Sano 1963); titanium dioxide has carcinogenic activity in the rat lung (Heinrich et al. 1995; Xu et al. 2010). Such chronic toxicity data will have more impact on risk assessment of nZnO.

Since nZnO induces inflammatory reaction, ROS production, and genotoxicity, which are implicated in cancer development, in the present study, we tested the lung carcinogenicity of nZnO by an initiation–promotion protocol using human c-Ha-*ras* proto-oncogene transgenic (H*ras* 128) rats, which have the same susceptibility to chemically induced lung carcinogenesis as their parent wild-type rats, but are highly susceptible to mammary tumor induction (Tsuda et al. 2005). The results indicated that nZnO did not have promotion effect on DHPN-induced lung and mammary carcinogenesis and caused reversible EHTB and FAIP.

Materials and methods

Animals

Forty-three female transgenic rats carrying the human c-Ha-RAS proto-oncogene (H*ras*128 rats) and 42 female wild-type Sprague–Dawley rats were obtained from CLEA Japan Co., Ltd. (Tokyo, Japan). The animals were housed in the Animal Center of Nagoya City University Medical School and maintained on a 12-h light/12-h dark cycle and received Oriental MF basal diet (Oriental Yeast Co. Ltd., Tokyo, Japan) and water ad libitum. The study was conducted according to the Guidelines for the Care and Use of Laboratory Animals of Nagoya City University Medical School, and the experimental protocol was approved by the Institutional Animal Care and Use Committee (H22M-19).

Preparation, characterization of nZnO suspensions, and administration of nZnO to the lung

Zinc oxide particles (CAS No. 1314-13-2, MZ-500, without coating, with a mean primary diameter of 25 nm) were obtained from Tayca Cooperation, Osaka, Japan. The particles were suspended in 0.1 % Tween 20 saline at 250 or 500 μg/ml. The suspension was sonicated for 20 min to prevent aggregate formation.

Characterization of nZnO was conducted as follows: the shape of nZnO in the suspensions was imaged by transmission electron microscopy (TEM); element analysis was performed by an X-ray microanalyzer (EDAX, Tokyo, Japan), after aliquots of nZnO were loaded on a carbon sheet; the size distribution of nZnO in the 500 μg/ml suspension was analyzed using a Particle Size Distribution Analyzer (Shimadzu Techno-Research, Inc., Kyoto, Japan). The characterization results are shown in Figure S1.

Before being administrated to rats, the nZnO suspensions were further sonicated for 20 min. 0.5 ml of the nZnO suspensions was administrated to the lung by intra-pulmonary spraying (IPS) as described previously (Xu et al. 2010).

Carcinogenicity study

The carcinogenic activity of nZnO was assessed in female H*ras*128 rats using an initiation–promotion protocol by which we used previously to evaluate lung and mammary carcinogenicity of titanium dioxide nanoparticles (Xu et al. 2010). Briefly, three groups of 10–11 female H*ras*128 rats aged 6 weeks were given 0.2 % DHPN (Wako Chemicals, Co., Ltd. Osaka, Japan) in the drinking water for 2 weeks, and Groups 4 and 5 (6 rats each) were given drinking water without DHPN. Two weeks later, Group 1 and Group 4 were administered 0.1 % Tween 20 saline, and Group 2, Group 3, and Group 5 were administered 250, 500, and 500 μg/ml nZnO suspensions by IPS once every two weeks from the end of week 4 to week 16, a total of 7 times. The total amounts of nZnO administered to Groups 1, 2, 3, 4, and 5 were 0, 0.875, 1.75, 0, and 1.75 mg/rat, respectively. The dosing was determined according to the permissible exposure limit for zinc oxide particles of the Occupational Safety and Health Administration (OSHA) (see Discussion). Three days after the last treatment, animals were killed and the organs (brain, lung, liver, spleen, kidney, mammary gland, ovaries, uterus, and neck lymph nodes) were fixed in 4 % paraformaldehyde in PBS buffer adjusted to pH 7.3 and processed for histological examination and transmission electron microscopy (TEM).

Light microscopy, polarized light microscopy, and transmission electron microscopy

Hematoxylin–Eosin (H&E)-stained pathological slides of the lung and other major organs were used to observe nZnO with a light microscope and polarized light microscope (PLM) (Olympus BX51N-31P-O polarized light microscope, Tokyo, Japan) at 1,000× magnification. Localization of the illuminated particles was confirmed in the same H&E-stained sections after removing the polarizing filter.

Paraffin blocks were deparaffinized and embedded in epon resin and processed for nZnO observation and zinc element analysis, using a JEM-1010 transmission electron microscope (TEM) (JEOL, Co. Ltd, Tokyo, Japan) equipped with an X-ray microanalyzer (EDAX, Tokyo, Japan).

Immunohistochemistry and Azan–Mallory staining

PCNA was detected using an anti-PCNA monoclonal antibody (Clone PC10, Dako Japan Inc., Tokyo, Japan). The antibody was diluted 1:200 in blocking solution and applied to deparaffinized slides, and the slides were incubated at 4 °C overnight. The slides were then incubated for 1 h with biotinylated species-specific secondary antibodies diluted 1:500 (Vector Laboratories, Burlingame, CA) and visualized using avidin-conjugated horseradish peroxidase complex (ABC kit, Vector Laboratories). To assess lung fibrosis, paraffin-embedded slides were deparaffinized, and collagen fibers were visualized by Azan–Mallory staining.

Reversibility study and effects of $ZnCl_2$ solution

To assess whether nZnO-induced terminal bronchiolar epithelial hyperplasia, interstitial pneumonitis, and lung fibrosis are reversible, we conducted reversibility experiments. Seven groups of 5 female wild-type Sprague–Dawley rats aged 10 weeks were administrated 0.5 ml of 0.1 % Tween 20 saline or 500 μg/ml nZnO suspension by IPS 2 times per week for 4 weeks. Group 1 was treated with 0.1 % Tween 20 saline and killed 1 day after the last IPS. Groups 2–7 were treated with 0.5 ml of 500 μg/ml nZnO suspension and killed at 1 day and 2, 4, 6, 8, and 12 weeks after the last IPS. For the comparison of the effects of zinc ion and nZnO, Group 8 was treated with 0.5 ml of 6.17 mM $ZnCl_2$ solution (the molecular amount is equal to that of 500 μg/ml nZnO suspension) by IPS at the same frequency and time period as the nZnO groups and killed 1 day after the last IPS. The left lung was cut into pieces and frozen in liquid nitrogen for biochemical analysis, and the right lung was processed for histological examination. Other major organs were excised for histological examination, and the blood was collected for cytological and biochemical analysis.

Gene expression analysis

The left lungs from Groups 1, 2, and 8 in the reversibility study described above were used for isolation of RNA. RNA was isolated by using TRizol reagent (Invitrogen of Life Technologies, CA).

For microarray analysis, 1 μg RNA from each rat of Group 1 was combined and 1 μg RNA from each rat of Group 2 was combined. The quality of the 2 mixtures of RNA samples was assessed and quantified using the Agilent 2100 BioAnalyzer RNA Nano chip system (Agilent Technologies, CA) prior to further manipulation. Microarray analysis was conducted by the 3-D Gene Chip (Toray Industries Inc., Kanagawa, Japan), and a total of 20,000 genes were analyzed. Microarray-based pathway analysis was performed by Toray Industries Inc., Kanagawa, Japan.

For reverse transcription-PCR (RT-PCR) and real-time PCR, first-strand cDNA synthesis from 1 μg of RNA was performed using SuperScript™ III First-Strand Synthesis System (Invitrogen of Life Technologies, CA) according to the manufacturer's instructions. Primers are as follows: forward primer, 5′-TAGAATCGAGGTGCACAGGAGT-3′, reverse primer, 5′-TATTCCAGCAGGCTGTCAAAGA-3′, product size, 228 bp for Orm1; forward primer, 5′-AAGTGGAGGAGCAGCTGGAGTGG-3′, reverse primer, 5′-CCAAAGTAGACCTGCCCGGACTC-3′, product size, 155 bp for Tnfa, and forward primer, 5′-AGCCATGTACGTAGCCATCC-3′, reverse primer, 5′-CTCTCAGCTGTGGTGGTGAA-3′, product size, 228 bp for Actb. RT-PCR was conducted using an iCycler (BioRad Life Sciences, CA) as follows: 95 °C 20 s, 60 °C 20 s, 72 °C 30 s, 30 cycles for Orm1; 95 °C 20 s, 60 °C 20 s, 72 °C 20 s, 25 cycles for Tnfa, and 95 °C 20 s, 60 °C 20 s, 72 °C 30 s, 15 cycles for Actb. Real-time PCR analysis of Orm1 and Tnfa gene expression was performed with the 7300 real-time PCR system (Applied Biosystem, CA) using the premix reagent Power SYBR Green PCR Master Mix (Applied Biosystem, CA) according to the manufacturer's instructions. The Actb gene was used as the normalizing reference gene.

Determination of zinc ion

For detection of Zn^{2+} content in the lung tissue, 50–100 mg of the frozen lung tissues from the reversibility study described above were thawed at room temperature, rinsed with cold PBS 3 times, and homogenized for 30 s at the highest speed in 1 ml of T-PER, tissue protein extraction reagent (Pierce, Rockford, IL), with Polytron R PT 2100 homogenizer (Capitol Scientific Inc., TX). The homogenates were clarified by centrifugation at 10,000×g for 15 min at 4 °C, and the supernatants were used for Zn^{2+}

detection. Zn^{2+} detection was performed using QuantiChrom™ Zinc Assay kit (BioAssay Systems, CA) according to the manufacturer's instructions.

In vitro nZnO dissolution assay

5 μl of 500 μg/ml nZnO suspension (2.5 μg/tube) and increasing amounts of 1 mg/ml human α 1 acid glycoprotein (Sigma-Aldrich, product number G9885) or bovine serum albumin (Sigma-Aldrich, product number A2058) were added to microtubes, and the total volume of each tube was adjusted to 100 μl with 0.1 % Tween 20 saline. The final protein concentration of human α 1 acid glycoprotein or bovine serum albumin was 0, 100, 200, 300, 400, and 500 μg/ml. The tubes were then incubated at 37 °C for 2 h. The nZnO particles were removed by centrifugation at 10,000×*g* for 5 min, and Zn^{2+} concentration in the supernatants was determined as described above.

In vitro cytotoxicity assay

The induction and preparation of rat primary alveolar macrophages (PAM) has been described (Xu et al. 2010). 5×10^3 PAMs, 1×10^3 A549 cells (human lung adenocarcinoma cell line), and 2×10^3 CCD34 cells (human lung fibroblast cell line) were seeded into 96-well culture plates and cultured overnight in 100 ml of RPMI 1,640 containing 10 % FBS. The cells were added with nZnO suspension or ZnCl2 solution to final concentrations of 0, 1, 5, or 25 μg/ml of nZnO and 0, 12.3, 61.7, or 308.6 nM of ZnCl2 (1, 5, and 25 μg/ml of nZnO are equal to 12.3, 61.7, and 308.6 nM of ZnCl2, respectively, in the amount of zinc element) and incubated for another 72 h. The cell viability was then determined using the Cell Counting Kit-8 (Dojindo Molecular Technologies, Rockville, MD) according to the manufacturer's instruction.

Statistical analysis

Statistical analysis was performed using ANOVA. Statistical significance was analyzed using a two-tailed Student's *t*-test. A p value of <0.05 was considered to be significant.

Results

Carcinogenesis study in H*ras*128 rats

DHPN-induced lung alveolar cell hyperplasia and adenoma development was used for the end point observation to assess the carcinogenicity of nZnO in our medium-term assay. As shown in Table 1, the incidence and multiplicity (number/cm^2 lung tissue section) of

Table 1 Effect of nZnO on lung proliferative lesions in H128-*ras* rats

Treatment	No. of rats	DHPN-induced proliferative lesions						DHPN-independent EHTB[a]	
		ACH[a]		Ade[a]		ACH + Ade		Inc. (%)	Multiplicity[b] (no./cm^2 lung)
		Inc.[a] (%)	Multiplicity[b] (no./cm^2 lung)	Inc. (%)	Multiplicity[b] (no./cm^2 lung)	Inc. (%)	Multiplicity[b] (no./cm^2 lung)		
DHPN + vehicle	11	11 (100)	2.43 ± 1.29	2 (18.1)	0.09 ± 0.20	11 (100)	2.52 ± 1.26	0 (0)	0
DHPN + 250 μg/ml nZnO	10	10 (100)	1.64 ± 1.09	3 (30.0)	0.12 ± 0.19	10 (100)	1.76 ± 1.03	7 (70)	0.86 ± 0.86 **
DHPN + 500 μg/ml nZnO	10	10 (100)	1.83 ± 1.05	5 (50.0)	0.30 ± 0.31	10 (100)	2.13 ± 1.23	10 (100)	4.93 ± 1.95 ***
Vehicle	6	0	0	0	0	0	0	0	0
500 μg/ml nZnO	6	2 (33.3)	0.16 ± 0.26	0	0	2 (33.3)	0.16 ± 0.26	6 (100)	3.91 ± 1.29 ***

[a] ACH, Ade, EHTB, and Inc. are abbreviations for alveolar cell hyperplasia, adenoma, epithelial hyperplasia of terminal bronchioles, and incidence, respectively

[b] Multiplicity is expressed as mean ± s.d

** and *** represent p values <0.01 and 0.001, respectively, versus DHPN + vehicle or vehicle

alveolar cell hyperplasia and adenoma in the groups treated with nZnO were not significantly different from the DHPN alone group. In the rats which received nZnO treatment without prior DHPN treatment, alveolar cell proliferation foci, recognized as thickening of the alveolar wall with proliferative alveolar epithelium, were observed, but significant differences from the saline group were not observed. In the mammary gland, significant inter-group difference in incidence and multiplicity of mammary tumors was also not observed (data not shown).

A notable lesion induced in all the nZnO-treated groups was epithelial hyperplasia of terminal bronchioles (EHTB). The EHTB lesions had increased cell density, often with the epithelial cells arranged in 1–3 layers, and partly extended bronchiolar structures with transition to the normal

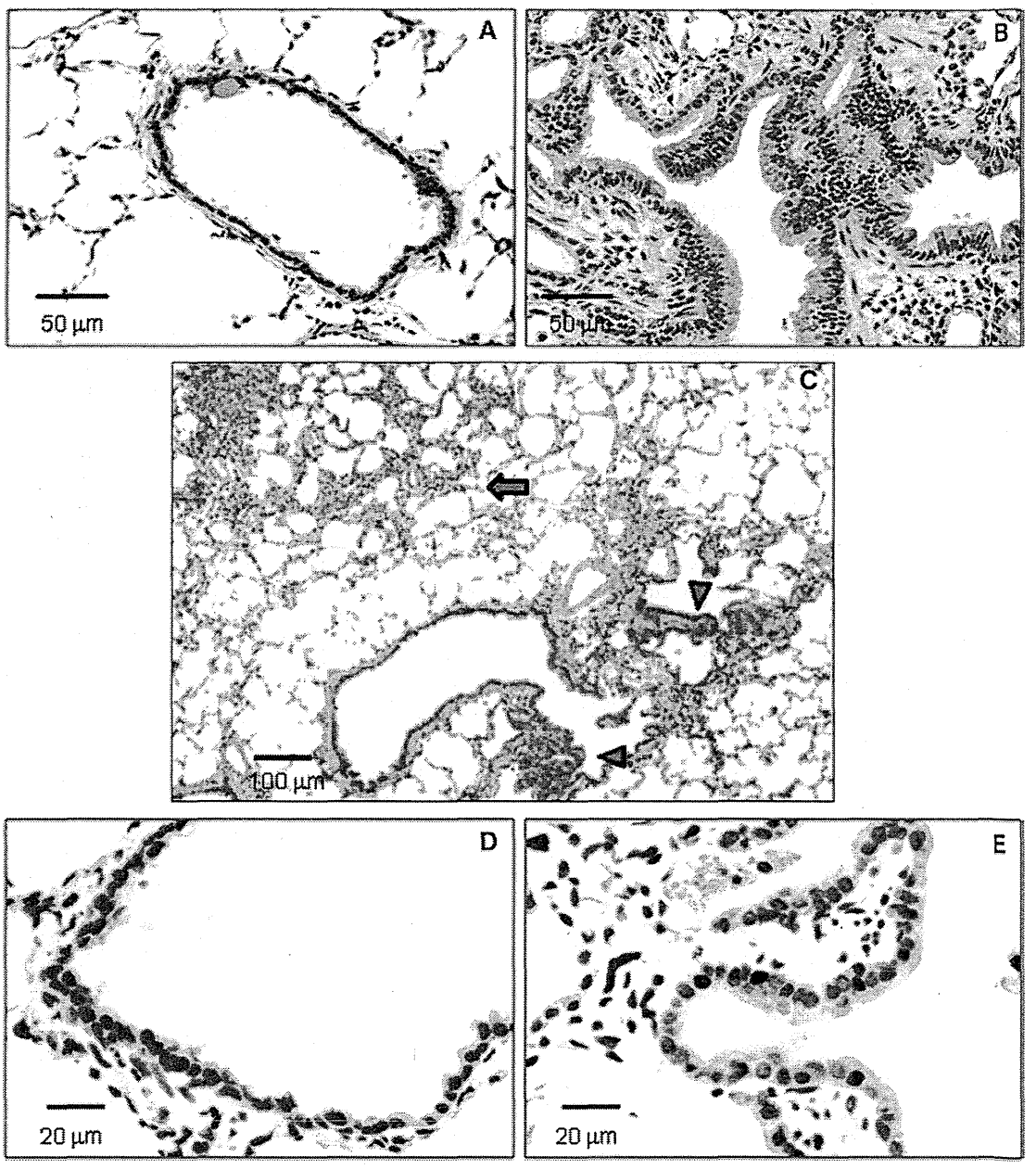

Fig. 1 Induction of EHTB by nZnO. **a** representative normal terminal bronchiolar epithelium (NTBE); **b** EHTB in H&E-stained slides; **c** images and localizations of DHPN-induced alveolar hyperplasia (*arrow*) and nZnO-induced EHTB (*arrow heads*); **d** images of PCNA immunostaining in NTBE; and **e** in EHTB

terminal bronchioles (Fig. 1a, b). The EHTB lesions were independently localized from the DHPN-induced alveolar cell hyperplastic lesions (Fig. 1c). The incidences and multiplicity (number/cm^2 lung tissue section) of EHTB in the groups treated with nZnO were significantly increased compared with that of the DHPN alone group. The increase was dose-dependent (Spearman rank correlation test, $p < 0.001$) (Table 1). Immunostaining with proliferating cell nuclear antigen (PCNA) indicated that proliferating bronchiolar epithelial cells were preferentially found in the EHTB lesions, but rarely found in the normal terminal bronchial epithelial areas (Fig. 1d, e).

Another lesion found in the groups treated with nZnO, and also independent of DHPN treatment, was interstitial pneumonitis (Fig. 2a). The lesion was usually associated with fibrosis of various thicknesses of the septal wall extruding into the alveolar structure (blue staining in Fig. 2b). Quantitative analysis indicated a significant increase in the fibrotic area in the rats treated with nZnO compared with that of rats treated with DHPN alone (Fig. 2c), and the increase was dose-dependent (Spearman rank correlation test, $p < 0.001$). In addition, the EHTB lesions often occurred near or within interstitial pneumonitis areas.

Light microscopic observation of the alveoli of the rats treated with nZnO showed infiltration of numerous macrophages mixed with a few neutrophils, eosinophils, and lymphocytes (data not shown). The nZnO particles were not found in any of the alveolar macrophages; these macrophages contained numerous vacuolar vesicles in the cytoplasm (Fig. 2d). Transmission electron microscopic (TEM) observation showed that nZnO particles were not found within the vacuolar vesicles (Fig. 2e) or in any alveolar tissue cells (Fig. 2f). The absence of a zinc peak was confirmed by elemental scanning with TEM-X-ray microanalysis (Figure S2). nZnO particles were also not detected under polarized light microscope observation. This feature was in contrast with titanium dioxide nanoparticles which were clearly observed in alveolar macrophages (Figure S3).

Reversibility of EHTB and FAIP in wild-type rats

As in the H*ras*128 transgenic rats, nZnO induced EHTB and FAIP in wild-type Sprague–Dawley (SD) rats (Fig. 3a), and nZnO was not found in the lung tissue. nZnO-induced EHTB and FAIP gradually regressed with time (Fig. 3a), and the number of EHTB foci per square centimeter lung tissue section decreased from 9.81 ± 1.42 at day 1 to 0.06 ± 0.13 at week 12 after cessation of nZnO exposure (Fig. 3b). The total Zn^{2+} content in the lung tissue also gradually decreased (Fig. 3c) and was positively correlated with the number of EHTB ($r = 0.96$ by Pearson correlation test).

Microarray analysis

Microarray analysis of the lung tissue indicated that nZnO treatment up-regulated the expression of 738 genes and down-regulated the expression of 267 genes (data not shown). The up-regulated inflammation-associated genes included chemotactic chemokines such as Cxcl5, Cxcl11, Ccl7, Cxcl2, Ccl2, and Cxcl1, proinflammatory cytokines such as Tnfa and Il6, and the acute-phase reactant Orm1 (Table S1). Pathway analysis showed an increase in inflammatory responses in which macrophages and TNFα play a central role (Figure S4). The gene expression profiling was consistent with the strong inflammatory responses in the lung observed by histological examination. Other pathways up-regulated by nZnO included classical complement activation pathway, matrix metalloproteinase pathway, cholesterol biosynthesis pathway and striated muscle contraction pathway, and treatment of nZnO down-regulated the adipogenesis pathway (data not shown).

Effects of $ZnCl_2$ solution on the lung of wild-type rats

To check whether the nZnO-induced EHTB and FAIP were due to dissolution of nZnO to Zn^{2+}, we administered $ZnCl_2$ solution (the molecular amount is equal to that of 500 μg/ml nZnO suspension) to the lung of rats by IPS. The lesions were histologically similar to those observed in the nZnO-treated rats (Fig. 4a, b, c). Quantitative analysis of EHTB indicated that the number of EHTB induced by $ZnCl_2$ solution and nZnO was comparable (Fig. 4d).

To examine whether Zn^{2+} and nZnO have the same underlying molecular mechanisms, two genes, Tnfa and Orm1, which were determined to be up-regulated in the nZnO-treated rats by microarray analysis, were chosen for gene expression analysis. These genes were chosen because Tnfa-encoded tumor necrosis factor alpha is a multifunctional proinflammatory cytokine involved in a variety of acute and chronic inflammatory responses, and Orm1-encoded alpha 1 acid glycoprotein (AGP) is an acute-phase protein usually synthesized by hepatocytes in response to trauma, infection, and inflammation (Fournier et al. 2000). RT-PCR (Fig. 4e) and real-time PCR (Fig. 4f) showed that treatment with both $ZnCl_2$ solution and nZnO increased the expression of Tnfa and Orm1 genes in the lung tissue, with a little higher induction in the $ZnCl_2$ solution treated rats. Similarly, increased expression of Orm1 genes was found in primary alveolar macrophages exposed to nZnO in vitro (Fig. 4g). Interestingly, addition of human AGP to nZnO suspension dose-dependently promoted dissolution of nZnO from 59.1 nmol/ml (19.7 % dissolved,

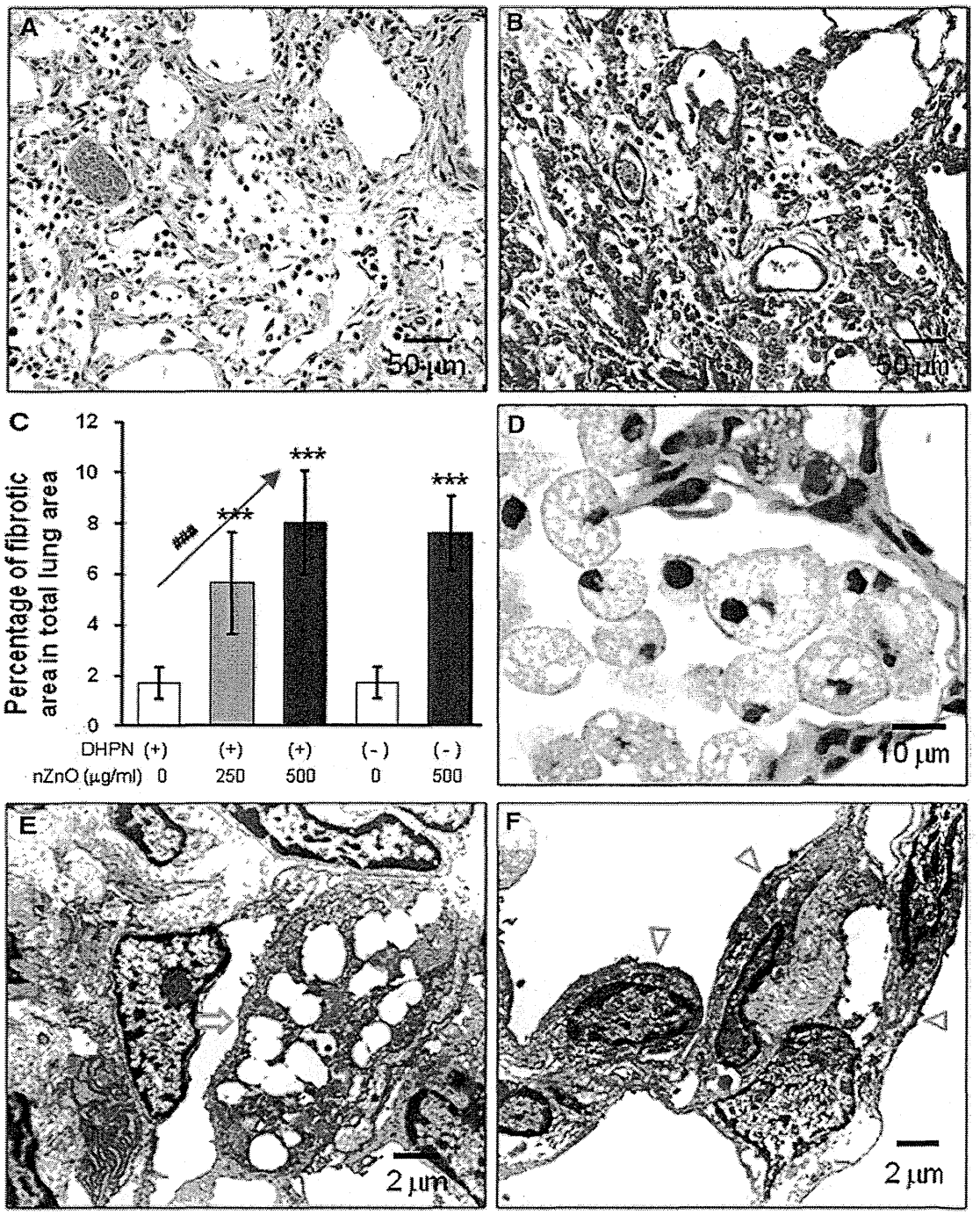

Fig. 2 Induction of FAIP and observation of nZnO particles. **a** representative image of FAIP in rats treated with nZnO; **b** image of Azan–Mallory staining in the lung of rats treated with nZnO, showing collagen fibers; **c** percentage of the fibrotic area in total lung tissue area. ***<0.001 by two-tailed Student's *t*-test versus the vehicle group; and ###$p < 0.001$ by Spearman rank correlation test. **d** image showing alveolar macrophages with vacuous phagocytosis vesicles; **e** and **f** TEM images showing alveolar macrophages (*arrow*) and epithelium (*arrow heads*), no nZnO particles being observed

without addition of AGP) to 117.3 nmol/ml (39.1 % dissolved after addition of 500 μg/ml of AGP), while addition of bovine serum albumin (BSA) had little effect on dissolution of nZnO (Fig. 4h). Exposure of both nZnO and $ZnCl_2$ solution resulted in dose-dependent cell death in vitro (Figure S5).

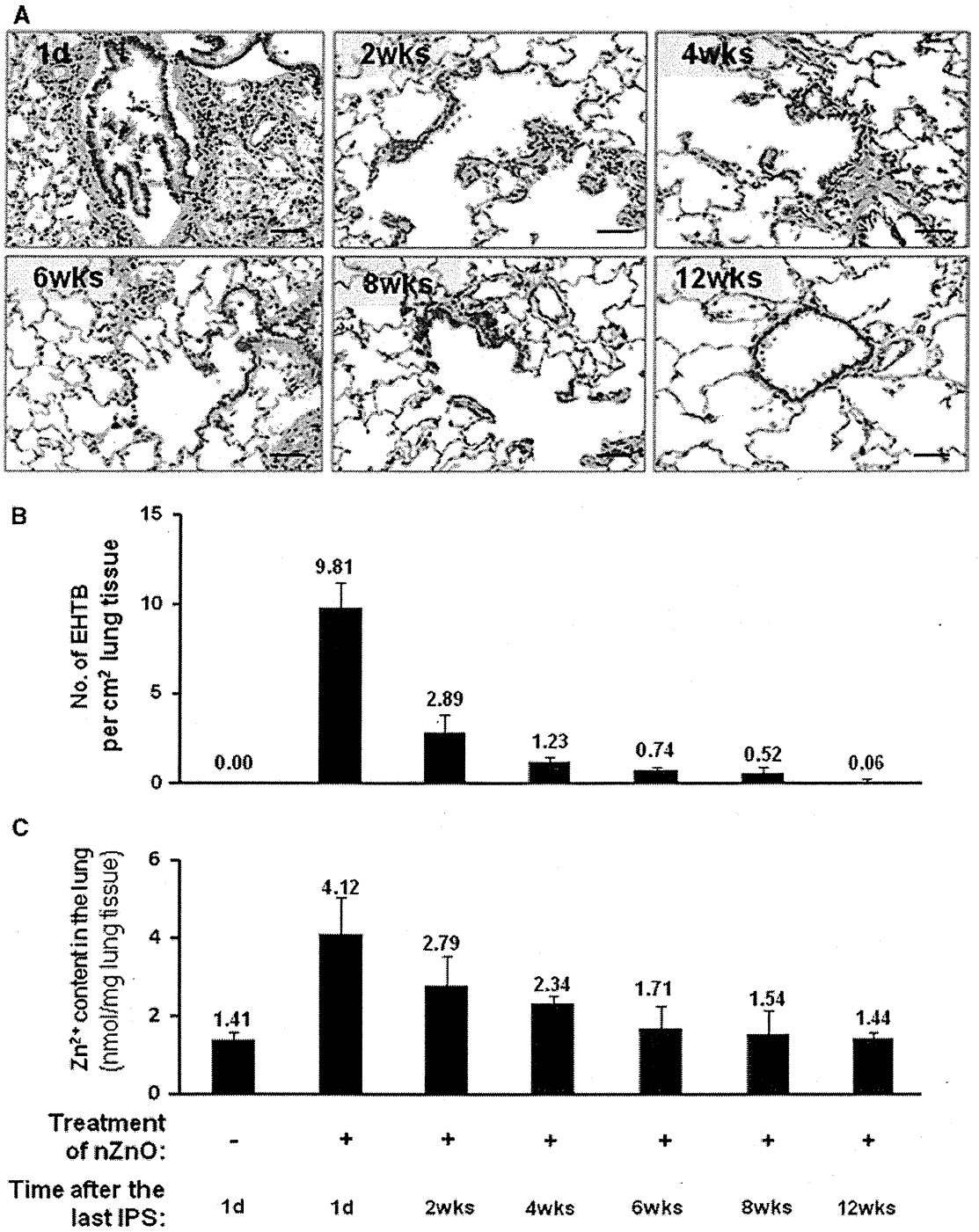

Fig. 3 nZnO-induced EHTB and FAIP are reversible. Wild-type rats were treated with 500 μg/ml nZnO by IPS 2 times/week for 4 weeks and killed at different time points of 1 day (1d) and 2, 4, 6, 8, and 12 weeks (wks) after the last IPS. **a** histological images of the lung tissues; **b** number of EHTB per cm^2 lung tissue and **c** Zn^{2+} content in the lung tissues at different time points. *Bars* = 50 μm

Effects of nZnO particles and $ZnCl_2$ solution on other organs and serum of wild-type rats

Obvious lesions and macrophages containing vacuolar vesicles were not found in other major organs including the liver, kidney, spleen, or brain by histological examination (data not shown). The results of blood cell examination are shown in Table S2: The only changes were increased proportions of monocytes and eosinophils that were rapidly recovered within 2 weeks post exposure. Biochemical

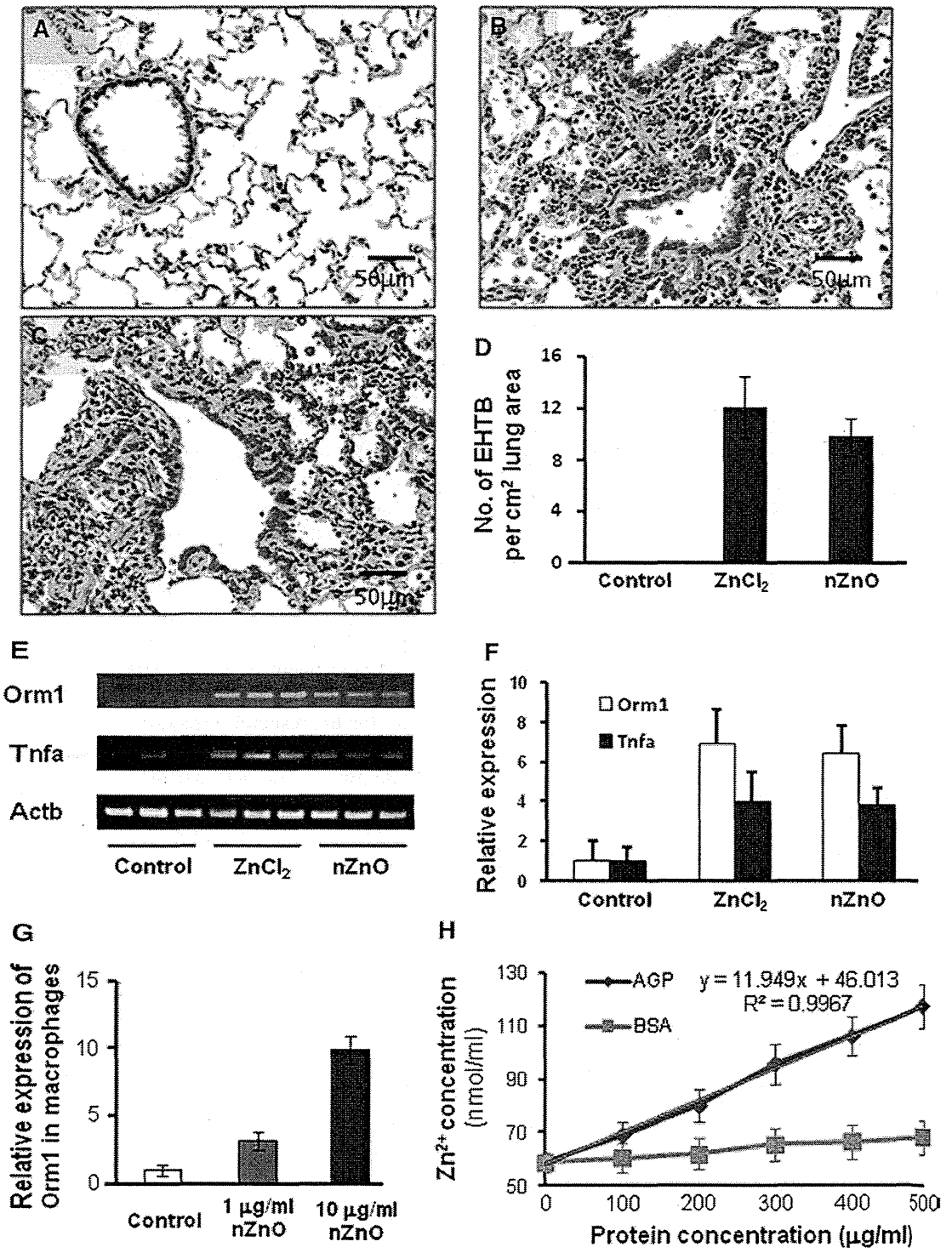

Fig. 4 Similar effects of $ZnCl_2$ solution and nZnO in induction of EHTB and FAIP in wild-type rats. **a** H&E-stained slides of the lungs of rats treated with vehicle; **b** with nZnO; and **c** with $ZnCl_2$ solution, showing EHTB and FAIP; **d** comparable number of EHTB per square centimeter of the lung tissues induced by treatment of $ZnCl_2$ and nZnO; **e** gene expression determined by RT-PCR of Orm1 and Tnfa, with Actb gene as an internal control; **f** real-time PCR analysis of gene expression of Orm1 and Tnfa, which was normalized with Actb expression; **g** induction of Orm1 expression in primary alveolar macrophages exposed to nZnO; and **h** effect of human alpha 1 acid glycoprotein (AGP) and bovine serum albumin (BSA) on dissolution of nZnO in vitro

examination of serum markers for tissue and organ injuries indicated no significant changes compared to the vehicle group (Table S3). Administration of nZnO or $ZnCl_2$ to the lung led to a transient increase in serum Zn^{2+} concentration which returned to normal levels within 2 weeks after administration. The elevated serum Zn^{2+} did not affect the homeostasis of the other ions examined (Table S4).

Discussion

In vivo nanomaterial toxicity usually implicates oxidative stress, inflammation (Nel et al. 2006), and other biological responses depending on the individual nanomaterial. In vitro assays related to carcinogenicity, such as mammalian cell transformation and gene mutation assays, cannot represent the complex in vivo processes of different biological alterations and are not always suitable for risk assessment of nanomaterial carcinogenicity. In the present study, we tested the carcinogenic activity of nZnO in H*ras*128 rats by an initiation–promotion protocol, by which we previously found promotion effect of nanosized titanium dioxide on DHPN-induced lung and mammary carcinogenesis (Xu et al. 2010). nZnO did not show any promotion effects on lung proliferative or neoplastic lesions, indicating that nZnO is not carcinogenetic. Also, nZnO did not promote DHPN-induced mammary carcinogenesis.

On the other hand, nZnO was found to induce EHTB in H*ras*128 rats and wild-type SD rats. EHTB is a proliferative lesion of the terminal bronchiolar epithelium. It should be noted that the localization of EHTB was independent from that of DHPN-induced alveolar cell hyperplasia. This observation clearly indicates that the DHPN-induced alveolar cell hyperplasia and EHTB have different etiology, the latter being induced by nZnO. We also observed 2 cases of alveolar cell hyperplasia out of 6 cases in the nZnO alone group. This is not significant and thus considered to be spontaneous or an inflammation-associated event. The EHTB lesions regressed when administration of nZnO was discontinued and completely disappeared after 12 weeks. Along with EHTB, the interstitial inflammatory changes often observed surrounding the EHTB lesions also regressed. Our data and other reports (Cho et al. 2011) indicate that the EHTB lesions do not progress directly to cancers but are reactive proliferation associated with inflammatory events. Similar reversible inflammatory changes in the bronchoalveolar lavage fluids by administration of nanoscale or fine ZnO particles via inhalation or intratracheal instillation have previously been reported (Warheit et al. 2009).

nZnO particles were not found in alveolar macrophages, in the lung tissue, or in other organs, suggesting that the particles were dissolved to Zn^{2+}. Accordingly, we conducted experiments to determine whether Zn^{2+} would induce similar lesions. $ZnCl_2$ solution induced closely similar lung lesions and gene expression profiles as nZnO, demonstrating that the observed lung lesions were caused by Zn^{2+}. This was confirmed by increased Zn^{2+} level in the lung and serum after administration of nZnO. Interestingly, treatment with nZnO up-regulated the expression of the Omrl gene in both the lung and the alveolar macrophages, and in vitro addition of Omrl-encoded AGP dose-dependently promoted nZnO dissolution. After Zn^{2+} was cleared from the lung, the EHTB and FAIP lesions disappeared, and this was evidenced by the positive correlation of EHTB number with Zn^{2+} content in the lung. Dissolution of nZnO has been reported to be particle size- and pH-dependent (Mudunkotuwa et al. 2012). Increased Omrl expression possibly alters the microenvironment of the alveolar macrophages and the lung which accelerates nZnO dissolution. The elevated Zn^{2+} from nZnO dissolution possibly interferes with zinc ion homeostasis and leads to cytotoxic effects (Kao et al. 2012).

According to OSHA, the permissible exposure limit for zinc oxide particles is 15 mg/m^3 of air for total dust and 5 mg/m^3 for the respirable fraction (http://www.osha.gov/SLTC/healthguidelines/zincoxide/recognition.html). The inhalation exposure limit per kilogram of body weight per day for the respirable fraction is 192 μg, calculated from 6,000 ml of minute respiratory volume and 8 working hours for a 75 kg body weight worker. The dosing in the carcinogenesis study of the present study was approximately 35.5 and 71 μg/kg body weight a day (calculated from 125 to 250 μg every two weeks for a 250 g rat) and is lower than the OSHA limit for humans. Since nZnO has more potential to be ionized than larger ZnO particles because of its higher surface area (Mudunkotuwa et al. 2012), this feature should be taken into regulatory consideration.

It has been estimated that engineered nanomaterials will become a $1 trillion enterprise by 2015 (Nel et al. 2006), and ensuring health and environmental safety is a challenging task to the nanotechnology industry. Among numerous engineered nanomaterials, metal based or carbon based, most of which have been shown to have toxic effects to at least some extent, nZnO is a promising nanomaterial for biomedical applications. The results of the present study indicate that, although nZnO induced reversible lung toxicity, it did not cause carcinogenic or chronic progressive inflammatory lesions. Also, since it is biodegradable to ions, nZnO is easily cleared from the body (Rasmussen et al. 2010). Our study also suggests that the toxic effects of nZnO can be further decreased if efforts such as proper dosing and surface coating are made to lower the Zn^{2+} release from nZnO.

In conclusion, treatment of nZnO by IPS did not promote lung and mammary carcinogenesis in our carcinogenesis model. Although nZnO induced EHTB and FAIP, the lesions regressed rapidly along with clearance of surplus Zn^{2+} from the lung and serum. Thus, from a toxicological viewpoint, under the present experimental conditions, exposure of the lung to nZnO does not cause progressive neoplastic development or chronic fibrosis in the lung. These findings will be helpful in evaluating of the safety of nZnO used in biomedical applications, in which its use is of rather short duration, although long-term studies including inhalation studies are required to assess their occupational and environmental health hazards.

Acknowledgments This work was supported by Health and Labor Sciences Research Grants (Research on Risk of Chemical Substance 21340601, H21-kagaku-ippan-008, H24-kagaku-ippan-009 and H22-kagaku-ippan-005) from the Ministry of Health, Labor and Welfare, Japan. We thank A. Iezaki for her excellent secretarial assistance for the work.

Conflict of interest The authors declare that they have no conflict of interest.

References

Antonini JM, Lewis AB, Roberts JR, Whaley DA (2003) Pulmonary effects of welding fumes: review of worker and experimental animal studies. Am J Ind Med 43:350–360

Baldwin S, Odio MR, Haines SL, O'Connor RJ, Englehart JS, Lane AT (2001) Skin benefits from continuous topical administration of a zinc oxide/petrolatum formulation by a novel disposable diaper. J Eur Acad Dermatol Venereol 15(Suppl 1):5–11

Cho WS, Duffin R, Howie SE, Scotton CJ, Wallace WA, Macnee W, Bradley M, Megson IL, Donaldson K (2011) Progressive severe lung injury by zinc oxide nanoparticles; the role of Zn2+ dissolution inside lysosomes. Part Fibre Toxicol 8:27–43

Deng X, Luan Q, Chen W, Wang Y, Wu M, Zhang H, Jiao Z (2009) Nanosized zinc oxide particles induce neural stem cell apoptosis. Nanotechnology 20:115101

Drinker CK, Fairhall LT (1933) Zinc in relation to general and industrial hygiene. Public Health Rep 48:955–961

Fine JM, Gordon T, Chen LC, Kinney P, Falcone G, Beckett WS (1997) Metal fume fever: characterization of clinical and plasma IL-6 responses in controlled human exposures to zinc oxide fume at and below the threshold limit value. J Occup Environ Med 39:722–726

Fournier T, Medjoubi NN, Porquet D (2000) Alpha-1-acid glycoprotein. Biochim Biophys Acta 1482:157–171

Heinrich U, Fuhst R, Rittinghausen S, Creutzenberg O, Bellmann B, Koch K, Levsen K (1995) Chronic inhalation exposure of wistar rats and two different strains of mice to diesel engine exhaust, carbon black, and titanium dioxide. Inhalation Toxicol 7:533–556

Hughes G, McLean NR (1988) Zinc oxide tape: a useful dressing for the recalcitrant finger-tip and soft-tissue injury. Arch Emerg Med 5:223–227

Hull MJ, Abraham JL (2002) Aluminum welding fume-induced pneumoconiosis. Hum Pathol 33:819–825

Kao YY, Chen YC, Cheng TJ, Chiung YM, Liu PS (2012) Zinc oxide nanoparticles interfere with zinc ion homeostasis to cause cytotoxicity. Toxicol Sci 125:462–472

Kermanizadeh A, Gaiser BK, Hutchison GR, Stone V (2012) An in vitro liver model–assessing oxidative stress and genotoxicity following exposure of hepatocytes to a panel of engineered nanomaterials. Part Fibre Toxicol 9:28

Lee J, Kang BS, Hicks B, Chancellor TF Jr, Chu BH, Wang HT, Keselowsky BG, Ren F, Lele TP (2008) The control of cell adhesion and viability by zinc oxide nanorods. Biomaterials 29:3743–3749

Mudunkotuwa IA, Rupasinghe T, Wu CM, Grassian VH (2012) Dissolution of ZnO nanoparticles at circumneutral pH: a study of size effects in the presence and absence of citric acid. Langmuir 28:396–403

Nel A, Xia T, Madler L, Li N (2006) Toxic potential of materials at the nanolevel. Science 311:622–627

Rasmussen JW, Martinez E, Louka P, Wingett DG (2010) Zinc oxide nanoparticles for selective destruction of tumor cells and potential for drug delivery applications. Expert Opin Drug Deliv 7:1063–1077

Sano T (1963) Pathology and pathogenesis of pneumoconiosis. Acta Pathol Jpn 13:77–93

Sayes CM, Reed KL, Warheit DB (2007) Assessing toxicity of fine and nanoparticles: comparing in vitro measurements to in vivo pulmonary toxicity profiles. Toxicol Sci 97:163–180

Tsuda H, Fukamachi K, Ohshima Y, Ueda S, Matsuoka Y, Hamaguchi T, Ohnishi T, Takasuka N, Naito A (2005) High susceptibility of human c-Ha-ras proto-oncogene transgenic rats to carcinogenesis: a cancer-prone animal model. Cancer Sci 96:309–316

Valdiglesias V, Costa C, Kilic G, Costa S, Pasaro E, Laffon B, Teixeira JP (2013) Neuronal cytotoxicity and genotoxicity induced by zinc oxide nanoparticles. Environ Int 55:92–100

Warheit DB, Sayes CM, Reed KL (2009) Nanoscale and fine zinc oxide particles: can in vitro assays accurately forecast lung hazards following inhalation exposures? Environ Sci Technol 43:7939–7945

Xia T, Kovochich M, Liong M, Madler L, Gilbert B, Shi H, Yeh JI, Zink JI, Nel AE (2008) Comparison of the mechanism of toxicity of zinc oxide and cerium oxide nanoparticles based on dissolution and oxidative stress properties. ACS Nano 2:2121–2134

Xu J, Futakuchi M, Iigo M, Fukamachi K, Alexander DB, Shimizu H, Sakai Y, Tamano S, Furukawa F, Uchino T, Tokunaga H, Nishimura T, Hirose A, Kanno J, Tsuda H (2010) Involvement of macrophage inflammatory protein 1 alpha (MIP 1 alpha) in promotion of rat lung and mammary carcinogenic activity of nanoscale titanium dioxide particles administered by intra-pulmonary spraying. Carcinogenesis 31:927–935

Yang H, Liu C, Yang D, Zhang H, Xi Z (2009) Comparative study of cytotoxicity, oxidative stress and genotoxicity induced by four typical nanomaterials: the role of particle size, shape and composition. J Appl Toxicol 29:69–78

The Journal of Toxicological Sciences (J. Toxicol. Sci.)
Vol.38, No.4, 619-628, 2013

Original Article

An improved dispersion method of multi-wall carbon nanotube for inhalation toxicity studies of experimental animals

Yuhji Taquahashi, Yukio Ogawa, Atsuya Takagi, Masaki Tsuji, Koichi Morita and Jun Kanno

Division of Cellular and Molecular Toxicology, Biological Safety Research Center, National Institute of Health Sciences, 1-18-1 Kamiyoga, Setagaya-ku, Tokyo 158-8501, Japan

(Received May 5, 2013; Accepted June 9, 2013)

ABSTRACT — A multi-wall carbon nanotube (MWCNT) product Mitsui MWNT-7 is a mixture of dispersed single fibers and their agglomerates/aggregates. In rodents, installation of such mixture induces inflammatory lesions triggered predominantly by the aggregates/agglomerates at the level of terminal bronchiole of the lungs. In human, however, pulmonary toxicity induced by dispersed single fibers that reached the lung alveoli is most important to assess. Therefore, a method to generate aerosol predominantly consisting of dispersed single fibers without changing their length and width is needed for inhalation studies. Here, we report a method (designated as Taquann method) to effectively remove the aggregate/agglomerates and enrich the well-dispersed singler fibers in dry state without dispersant and without changing the length and width distribution of the single fibers. This method is base on two major concept; liquid-phase fine filtration and critical point drying to avoid re-aggregation by surface tension. MWNT-7 was suspended in Tert-butyl alcohol, freeze-and-thawed, filtered by a vibrating 25 μm mesh Metallic Sieve, snap-frozen by liquid nitrogen, and vacuum-sublimated (an alternative method to carbon dioxide critical point drying). A newly designed direct injection system generated well-dispersed aerosol in an inhalation chamber. The lung of mice exposed to the aerosol contained single fibers with a length distribution similar to the original and the Taquann-treated sample. Taquann method utilizes inexpensive materials and equipments mostly found in common biological laboratories, and prepares dry powder ready to make well-dispersed aerosol. This method and the chamber with direct injection system would facilitate the inhalation toxicity studies more relevant to human exposure.

Key words: Multi-wall carbon nanotube, Dispersion, Metallic sieve, Tert-butyl alcohol, Sublimation, Critical point drying

INTRODUCTION

We previously reported that a certain make of multi-wall carbon nanotube (MWCNT) contained particles similar to asbestos fibers in size and shape, and was positive for mesotheliomagenesis in intraperitoneal injection studies using p53-heterozygous mice (Takagi *et al.*, 2008, 2012). The intraperitoneal injection study is a specialized method for the detection of mesotheliomagenic potential of inhaled fibrous materials (Pott *et al.*, 1994; Roller *et al.*, 1997; Poland *et al.*, 2008). For the assessment of general respiratory toxicity including non-cancerous endpoints, the inhalation studies are considered essential. As a surrogate for inhalation studies, pharyngeal aspiration and intratracheal spray methods are often used. However, in both methods, the suspension medium may modify the distribution and/or the toxicity of the test particles (Morimoto *et al.*, 2011; Oyabu *et al.*, 2011; Gasser *et al.*, 2012; Wang *et al.*, 2012). Dispersion methods without suspension media are reported. However, those are usually using, at least in part of the processes, rigorous sonication or mechanical milling resulting in certain degree of physiological changes in sample characteristics, such as shortening in length distribution of MWNCT (Muller *et al.*, 2005; Mitchell *et al.*, 2007; Ahn *et al.*, 2011). Changes in particle size and/or shape will also affect the nature

Correspondence: Jun Kanno (E-mail: kanno@nihs.go.jp)

and strength of toxicity of the test substances. Therefore, development of a dispersion method to generate the aerosol of concern without addition of chemicals and changes in particle dimensions is considered to be essential for the assessment of inhalation toxicity in humans.

Fibrous nanomaterial such as Mitsui MWNT-7 is a mixture of dispersed single fibers of various length and width, and their agglomerates and aggregates. When given as a mixture, the lung lesions were mainly seen as inflammatory and/or granulomatous lesions with various degree of fibrosis at the level of terminal bronchiole accompanying the aggregates and agglomerates. These lesions were considered to block and/or mask the changes induced by the single fibers that should have reached the alveolar ducts and alveoli (Warheit *et al.,* 2004; Muller *et al.,* 2005; Shvedova *et al.,* 2008; Porter *et al.,* 2009; Mercer *et al.,* 2011; Wang *et al.,* 2011). Therefore, assessment of the toxicity of single fibers needs well-dispersed sample without aggregate/agglomerate. In practical inhalation testing, the animal chamber air is rigorously agitated in order to ensure the homogeneity of aerosol in the chamber. Therefore, if the MWNT-7 as a mixture is used, the likelihood of aggregates/agglomerates reaching the nose of the animals is high. In contrast, human ambient air is less agitated; the aggregates/agglomerates may sediment away fast and dispersed single fibers may stay longer in the air to be inhaled by humans (Han *et al.,* 2008). In addition, humans have longer respiratory tract compared to rodents and may effectively filtered out aggregates/agglomerates before the air reaches the alveolar region.

Taking all into account, we concluded that it is essential to prepare a dispersed single fiber aerosol without aggregate/agglomerates, without additional chemical components, and without changes in size and shape of the single fiber component for the rodent inhalation studies in order to predict human inhalation toxicity. To date, one dispersion method is reported, i.e. the filtration system. Filtration by a sieve with its pore size smaller than the size of aggregates/agglomerate will not affect the size distribution of the single fibers (Kasai *et al.*, 2013). However, filtration in gaseous phase turns out to be ineffective in terms of yield of the filtrate. Filtration in liquid phase is much efficient (Mercer *et al.,* 2008; Tsuda, personal communication). However, in our experience, the difficulty is found in avoiding re-aggregation during the process of drying; the surface tension. To solve this problem, here we report a new improved dispersion method consisting of a combination of aqueous filtering and the concept of a drying method used for scanning electron microscopic (SEM) samples; the critical point drying.

MATERIALS AND METHODS

MWCNT, reagent and equipments

MWCNT (Mitsui MWNT-7) was kindly donated by Mitsui & Co., Ltd., Tokyo, Japan for use in toxicity studies (Takagi *et al.,* 2008). Tert-butanol (TB) of guaranteed reagent grade was used (CAS: 75-65-0, Kanto Chemical Co., Inc., Tokyo, Japan). Metallic Sieve (pore size 25 μm mesh, Seishin Enterprise Co., LTD., Tokyo, Japan) was used for filtration. Miniature coin type vibration motors used in cellular phones (Model FM34F, T.C.P. Co, Tokyo Japan; 13,000 rpm 1.8m²/sec) are attached to the extended filler rim (5cm in depth, custom-made, Seishin Enterprise Co., LTD.) of the metallic sieve (cf. Fig. 1c) to gain high yield of filtrate. Chemistry diaphragm pumps and pumping systems (Model; MD4C NT+AK+EK, Vacuubrand, Wertheim, Germany) was used for sublimation of the frozen TB suspension and recovery of TB. Glass wares such as funnel, filtering bottle, trap bottle and silicon stoppers (Sansyo Co., Ltd., Tokyo, Japan), laboratory bottles (Pyrex®, Asahi Glass Co. Ltd., Tokyo, Japan), were used.

Dispersion method ("Taquann" method)

An outline flowchart is shown in Fig. 1. TB (melting point 25.69°C) was heated up to 60°C by a mantle heater (Sibata Scientific Technology Ltd., Saitama, Japan). It is advised not to use water bath; TB is highly hygroscopic and becomes difficult to freeze and sublimate. A volume of 200 ml of TB and 0.2 g of MWCNT were transferred to a 500 ml laboratory bottle and agitated to make crude suspension. The bottle was put into an ice bath, occasionally shaken by hand, until the suspension starts to freeze and becomes sherbet-like half frozen state and kneaded by a stainless steel spatula until it becomes evenly gray without clear crystals of TB (Fig. 1a), and then kept overnight at -25°C. To the frozen suspension, 500 ml of TB pre-heated to 60°C, was added, capped and shaken hard until the liquefied suspension becomes evenly dark brown to gray in color (Fig. 1b). The bottle was further heated up to 60°C by a mantle heater and the suspension was immediately applied to vibrating metal sieve for filtration (Fig. 1c). The filtrate was collected through a funnel into a 1,000 ml laboratory bottle. Immediately after the filtration, approximately 1,500 ml of liquid nitrogen was poured onto the filtrate in the bottle to snap freeze the suspension (Fig. 1d). Then, the bottle was connected to the pumping system and vacuumed until TB was totally sublimated; leaving dispersed MWCNT (T-CNT for Taquann-treated MWCNT) in the bottle. The MWCNT was collected by a cyclone-suction bottle using conduc-

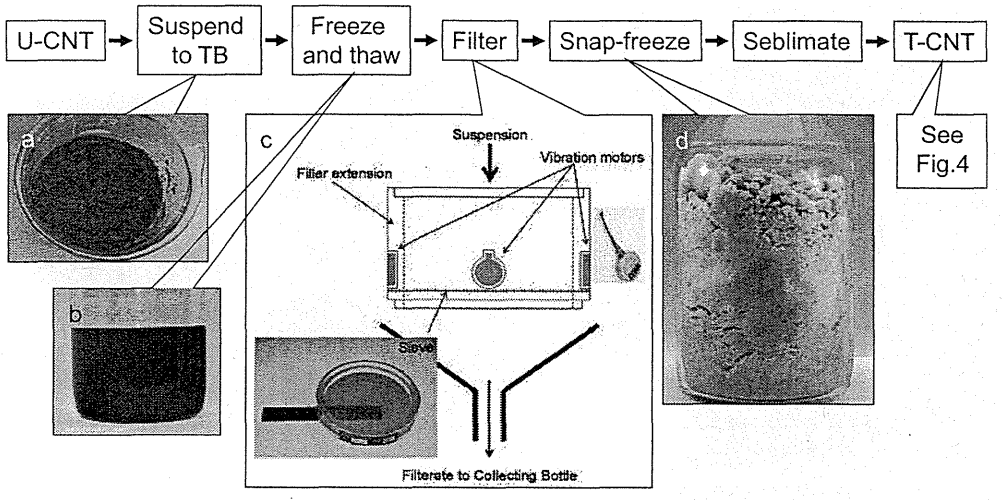

Fig. 1. Outline flowchart of the Taquann method. a) Half-frozen sherbet-like suspension of MWNT-7 kneaded (beaker was used for demonstration). b) Well-shaken liquefied suspension after adding 60°C TB (beaker was used for demonstration). c), Photograph of the sieve on a backlight box with a scale underneath (left inset), vibration motor (right inset), and a diagram of the filter unit with a filler extension and vibration motors. d) Snap-frozen filtrate.

tive silicon and aluminum tubing. In order to make a precise aliquot, a measured amount the collected T-CNT was resuspended to TB, and the suspension was aliquoted into proper containers, in this study into the newly designed cylindrical cartridge case (cf. Fig. 3), snap-frozen, and sublimated.

Aerosol generation system

An originally designed 105 L main exposure chamber (capacity of 16 mice per chamber), with a disposable electrostatic-free plastic bag inside, was prepared (Fig. 2, patent pending, manufactured by Sibata Scientific Technology Ltd.). Onto the plastic disposable top plate, a 20 L subchamber was connected with a 5 cm-diameter 10 cm long connecting pipe. To the subchamber, an injection port was connected, to which a newly designed cylindrical cartridge (manufactured by Sibata Scientific Technology Ltd.) containing dispersed T-CNT is loaded. The cartridge has a slide-valve air inlet at its base and four ejection holes at its top opening towards the subchamber lumen. The compressed air (0.8 M pascal) was injected five times with 0.2 sec duration and 10 sec interval to empty the T-CNT into the subchamber (Fig. 3). The carrier air flow from the subcamber to the main chamber was 15 L/min. Twenty-one cartridges were prepared for a two-hr exposure experiment, loading first two in 1 min for an initial boost and then one in every 6 min, resulting in generation of saw-tooth concentration wave with an average of 1.3 mg/m^3 (250 μg/cartridge) and 2.8 mg/m^3 (500 μg/cartridge).

Twelve C57BL/6NCrSlc male mice (SLC, Inc., Shizuoka, Japan), 10~11 weeks old, body weight of 23.8~30.8 g were placed in the cage suspended from the top plate of the inhalation chamber and exposed to 1 mg/m^3 of T-CNT for 2 hr a day for 5 days, lungs (excluding primary bronchi) were sampled and subjected to characterization of deposited fibers (see below).

The animal study was conducted in accordance with the Guidance for Animal Studies of the National Institute of Health Sciences under Institutional approval.

Real time particle counting and weight measurement

An optical particle counter (OPC) with a nominal detection limit of 300 nm (OPC-110GT, Sibata Scientific Technology Ltd.) and a condensation particle counter (CPC) with a nominal detection limit of 2.5 nm (ultrafine condensation particle counter 3776, Trust Science Innovation, MN, USA) were connected to the main chamber with a sample flow of 2.83 L (0.1cf) /min and 0.3 L/min respectively. The mass concentration of the chamber aerosol was calculated from the weight increase of polytetrafluoroethylene-glass fiber filter (Model T60A20, φ55mm, Tokyo Dylec Corp, Tokyo, Japan) after filtering the chamber aerosol by an Asbestos sampling pump (AIP-105, Sibata Scientific Technology Ltd.) at a rate of 1.5 L/min for 120 min (total of 180 L). Filter weight was measured by a microbalance (XP26V,

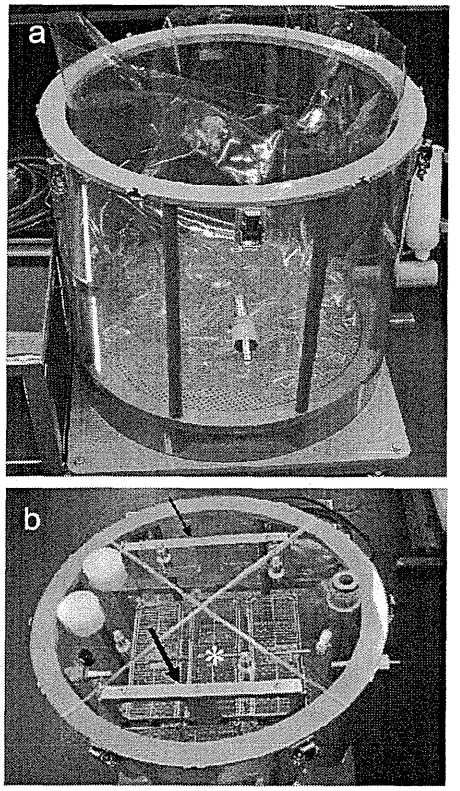

Fig. 2. Newly designed original inhalation chamber. a) Outer chamber and inner bag before top plate is in place. During operation, the space between the outer chamber and inner bag is negatively pressured to inflate the inner bag. B) Disposable top plate with tubing holes are placed on the chamber. The animal cages for 16 mice (asterisk) are suspended from the top place by a pair of hanger arms (arrows) (photo was taken without inner bag for better demonstration).

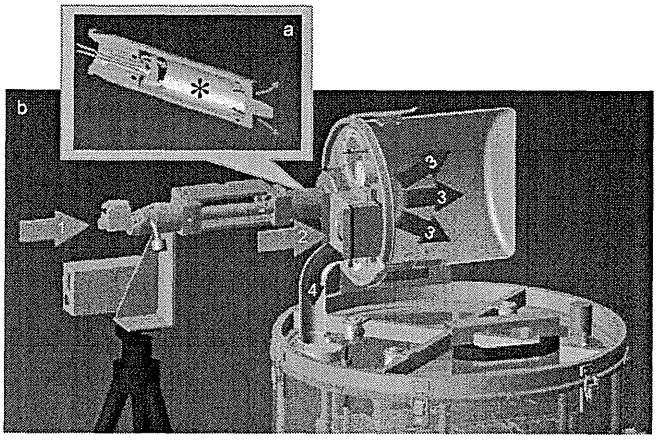

Fig. 3. A scheme of direct injection aerosol generation system. a) Upper inset shows the cut section of the injection cartridge (capacity; 23.5 ml). A slide valve opens when the cartridge is loaded to the subchamber. A measured amount of dispersed MWCNT is preloaded inside the cartridge shown in asterisk. b) Compressed air (Blue arrow 1) blows out the MWCNT through four small outlets of the cartridge into the subchamber (red arrows 3), where main flow air from the HEPA filtered inlet (blue arrow 2) mixes in. The air with the aerosol goes down the connection pipe to the main chamber (red arrow 4).

Mettler Toledo).

Characterization of the dispersed MWCNT

The T-CNT in TB suspension was mounted on a slide glass and observed under a light microscope using a pair of polarizing filters. Untreated MWCNT (U-CNT) from the bulk, 200 mg, was dispersed in to 500 ml of TB and sonicated for 30 min at 40W, 3.4 kHz (SU-3TH, Sibata Scientific Technology Ltd.) and observed.

A weight-measured aliquot of T-CNT was re-suspended, blotted on a Anopore™ Inorganic Aluminum Oxide Membrane Filters (Whatman GmbH, Dassel GE Healthcare, Hahnestrasse, Germany, pore size; 0.02 μm, φ13 mm, Anodisc 13) or a cellulose acetate/nitrocellulose membrane filter (MFTM- Millipore Membrane filters, 0.025 μm, φ13 mm, Merck Millipore, Billerica, MA, USA) and observed with a scanning electron microscope (SEM).

From the main chamber, the aerosol was collected at a rate of 5 L/min for 3 min on a Anopore™ Inorganic Aluminum Oxide Membrane Filters (Whatman GmbH, pore size; 0.1 um, Anodisc 25) joined to asbestos sampling pump (AIP-105, Sibata, Scientific Technology Ltd.). A scanning electron microscope (SEM) (VE-9800, Keyense Co., LTD., Osaka, Japan) was used for monitoring the details of the samples on the slide glasses and on the Anodiscs after osmium coating (HPC-1SW, Vacuum Device Inc., Ibaraki, Japan).

From the exposed mouse, lung lobes are collected and treated with lysis solution composed of 5 w/v% potassium hydroxide (Super Special Grade, Wako Pure Chemical Industries, Ltd., Osaka, Japan), 0.1w/v% Sodium dodecyl sulfate (SDS, for Biochemistry, Wako Pure Chemical Industries, Ltd.), 0.1 w/v% Ethylenediamine-N,N,N',N'-tetraacetic acid disodium salt dehydrate (EDTA 2Na, Dojindo laboratories, Kumamoto, Japan) and 2w/v% ascorbic acid (Super Special Grade, Wako Pure Chemical Industries, Ltd.) in ultra-pure water, dissolved at 80°C (Fig. 10b). Lung samples (approx. 200 mg) and 1.8 ml of

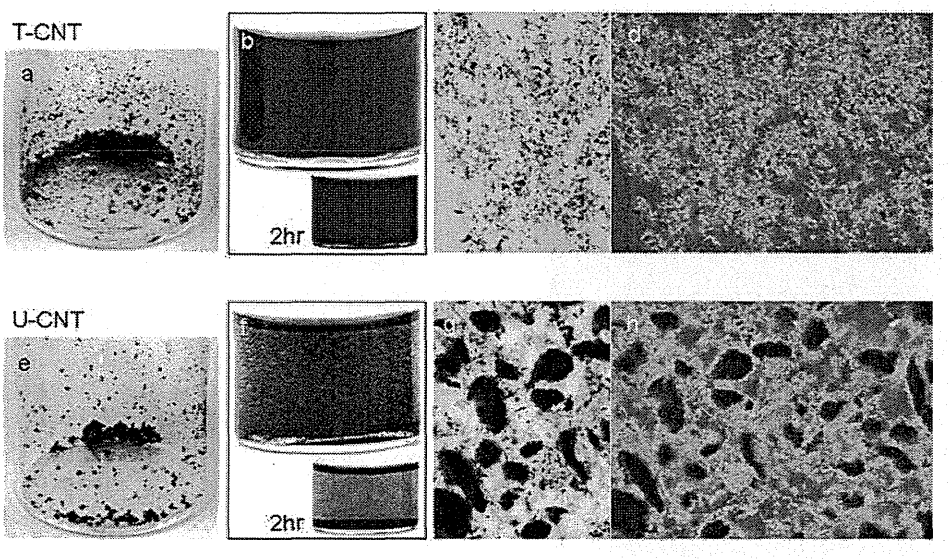

Fig. 4. Taquann-treated carbon nanotube (T-CNT) and untreated bulk carbon nanotube (U-CNT). a) final fine and dry powder of Taquann-treated MWCNT. b) Resuspended T-CNT to TB and placed for 5 min and 2 hr; T-CNT suspension is stable, compared to U-CNT, c) light microscopic view of the resuspended T-CNT on a slide glass, and d) under polarized light. e) course powder of U-CNT, f) Resuspended U-CNT to TB and placed for 5 min and 2 hr. g) light microscopic view of the resuspended U-CNT on a slide glass, and d) under polarized light. (diameter of the vials in a), b), e) and f) is 2.3 cm)

lysis solution in a centrifuge tube (DNA LoBindid tube 2.0 ml, Eppendorf, Hamburg, Germany) was incubated at 80°C for approx. 24 hr in an oven (HV-100, Funakoshi Co., Ltd., Tokyo, Japan), centrifuged at 20,000 g for 1 hr at 25°C (MX-207, Tomy Seiko Co., Ltd., Tokyo, Japan), and the pellet containing MWCNTs and SDS crystals was recovered. 1.8 ml of 70% ethanol was added to the tube and incubated at 80°C for 30 min to dissolve SDS crystals and centrifuged at 20,000 g for 1 hr at 25°C. 100 μl of 1w/w% Triton®X-100 (MP Biomedicals, Inc., Solon, OH, USA) was added to the pellet and dispersed by pipetting. One microliter of the suspension was placed on an inorganic aluminum oxide membrane filter (Anodisc 13, 0.02 μm φ13mm, Whatman GmbH) or the cellulose acetate/nitrocellulose membrane filter and filtrated on a funnel shape glass filter (SANSYO Co., LTD., Tokyo, Japan). The filter was dried at room temperature and osmium coated for SEM. For a reference of extraction efficiency, lung sample from untreated mouse was spiked with 1 μg T-CNT and measured alongside.

Lung tissue from eight mice were fixed with buffered 10% formalin (four with and four without inflation), paraffin embedded and processed routinely for H&E stained histology slides, and observed under a light microscope with or without polarizing filters (Olympus BX50 microscope with DP-70 image system, Olympus Corporation, Tokyo, Japan).

RESULTS

Characteristics of "Taquann"-dispersed MWCNT

Macroscopic and light microscopic views of the final product, the dried MWCNT after sublimation, i.e. "Taquann"-dispersed MWCNT (T-CNT) and, for comparison, untreated MWCNT from the bulk (U-CNT) are shown in Fig. 4. The powder of T-CNT is finer compared to U-CNT (Fig. 4a). The T-CNT resuspended very well to TB (Fig. 4b) and other solvents including 0.1 w/v% Sodium dodecyl sulfite and 0.1 w/v% Sodium dodecylbenzene sulfonate (not shown). Light microscopically, the resuspended T-CNT consists mostly of dispersed single fibers with smaller numbers of small aggregates corresponding to the mesh size of the metal sieve (Figs. 4c, 4d), whereas U-CNT was a mixture of large aggregates/agglomerates and single fibers among them (Figs. 4g, 4h). The T-CNT fibers slowly precipitated in the medium (cf. Figs. 4b and f), and are easily resuspended by gentle agitation. The yield of the T-CNT was approximately 5% of the U-CNT in weight. Re-filtration of the residue on the sieve resulted in negligible yield. The low power SEM views of the TB-resuspended T-CNT and U-CNT are shown in Fig. 5.